Analytical Methods

Accepted Manuscript

This article can be cited before page numbers have been issued, to do this please use: C. Rodriguez-Quijada, C. Lyons, C. Santamaria, S. Quinn, M. Tlusty, M. Shiaris and K. Hamad-Schifferli, *Anal. Methods*, 2020, DOI: 10.1039/D0AY00725K.

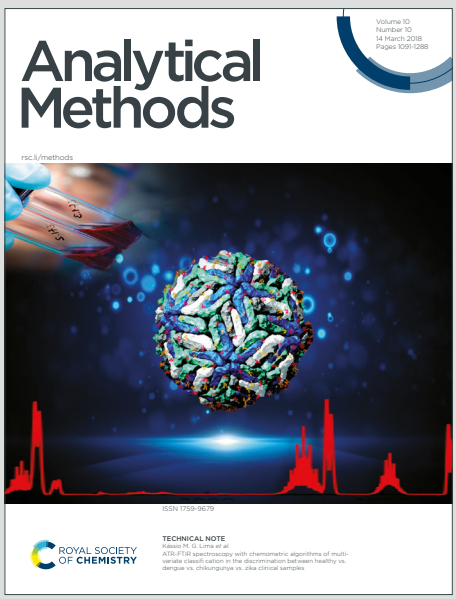

ROYAL SOCIETY OF CHEMISTRY

rsc.li/methods

View Article Online
DOI: 10.1039/D0AY00725K

ARTICLE

Optimization of paper-based nanoparticle immunoassays for direct detection of the bacterial pathogen *V. parahaemolyticus* in oyster hemolymph

Received 00th January 20xx,
Accepted 00th January 20xx

DOI: 10.1039/x0xx00000x

Cristina Rodriguez-Quijada,[a] Casandra Lyons,[b] Charles Santamaria,[b] Sara Quinn,[b] Michael Tlusty,[c] Michael Shiaris,[b] Kimberly Hamad-Schifferli[a,c]*

The detection of foodborne pathogens is critical for disease control and infection prevention, especially in seafood consumed raw or undercooked. Paper-based diagnostic tools are promising for rapid fieldable detection and provide a readout by eye due to the use of gold nanoparticle immunoprobes. Here we study different strategies to overcome these challenges in a real biological matrix, oyster hemolymph, for the detection of the pathogenic bacteria *Vibrio parahaemolyticus* (Vp). Nanoparticle surface chemistry, nitrocellulose speed and blocking, running steps, and antibody concentrations on the NP and nitrocellulose were all studied. Their effect on paper immunoassay signal intensity was quantified to determine optimal conditions, which enabled the detection of Vp directly from hemolymph below pathogenic concentrations.

Introduction

Diagnostic assays are critical tools for global health as they have the ability to rapidly identify diseases, toxins and pathogenic species that pose threats to humans. Diagnostics can provide information for decision making to control the spread of a disease, prevent infection, and enable disease surveillance. One diagnostic application area that is growing is food safety, where they can be used to diagnose food borne illnesses that pose major health hazards.[1, 2] Foodborne pathogens are predominantly bacterial pathogens, such as *Salmonella, Listeria, E. coli,* and Vibrio.[3] Vibrio is of particular concern as it is one of the major causes of food borne illnesses in the world, which is problematic for the consumption of raw or undercooked seafood such as oysters.[4, 5] In addition, it is pathogenic to important aquaculture products such as shrimp, causing early mortality syndrome (EMS).[2, 6] Vibrio contamination can cause significant economic repercussions, such as forcing the closure of oyster beds to clear out the pathogenic species, or the death of shrimp, which results in the loss of viable product. With climate change, warmer temperatures facilitate bacterial growth, extending seasons where it is unsafe to consume raw oysters and other seafood.[7]

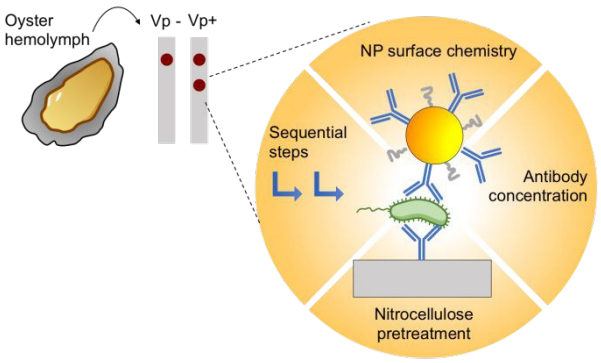

Figure 1. Schematic of the strategies used in this work on paper immunoassays for Vibrio.

Consequently, Vibrio contamination is a growing public health problem.

Because of distribution networks and the decentralized nature of food transport and consumption, food safety requires assays that are fieldable, rapid, and sensitive.[8-11] The gold standard for bacterial identification is PCR, which requires culturing and isolation of the bacteria from a sample. This process is time consuming and can take several days. In addition, the technique requires lab expertise, specialized reagents, and must be performed in a centralized lab, preventing deployment in the field.[3, 12]

Point of care (POC) diagnostics are promising solutions for bacterial detection, where the possibility of eliminating culture time can facilitate rapid response and the decision-making process.[8, 11] Lateral flow immunoassays (LFAs) and other

[a] Dept. of Engineering, University of Masschusetts Boston, 100 Morrissey Blvd., Boston, MA 02125, USA
[b] Dept. of Biology, University of Massachusetts Boston, 100 Morrissey Blvd., Boston, MA 02125, USA
[c] School for the Environment, University of Massachusetts Boston, 100 Morrissey Blvd., Boston, MA 02125 USA

paper-based tests are attractive as diagnostics because they can go from sample to answer within minutes and be operated by non-experts. [13-22] A sample fluid is added to the LFA, and if an antigen of interest is present, a color appears at the test area due to the presence of gold nanoparticles (Au NPs).[23] They rely on capillary action to drive the fluid through the paper membrane, so no external power is required to run the test. [24] Furthermore, paper is inexpensive to manufacture at large scale and, due to its robustness as a substrate, contributes to the portability of these assays.[25, 26]

However, one of the biggest impediments for POC assay performance are sample matrix and preparation issues.[27, 28] Real sample matrices are much more complex and challenging to work with than pure antigens in solution. Sample matrix effects are unpredictable, causing non-specific adsorption and aggregation, which can introduce false positives or negatives [29-31]. Oyster circulatory fluid, or hemolymph, has a high salt concentration and is a complex, heterogeneous solution, containing many different types of bacteria and proteins.[32] Most studies using LFAs for bacterial pathogen detection have focused on technology development, and typically explore only spikes into pure solutions, which are highly simplified compared to real samples.[33] Moreover, LFA sample preparation, when discussed, is predominantly focused on human biological fluids such as blood, serum, or urine. In comparison, food sample matrices are much more challenging. Food comes in a broad range of formats, where it can be in multiple phases such as mixtures of solids with liquids or slurries, and generally is not as well characterized as human biological fluids.

Issues of reproducibility and reliability already pose a challenge for LFA utility.[34] Thus, routes to improve assay performance in complex sample matrices are needed if we are to expand their use in food safety.[35] Because the signal in a paper immunoassay is due to the presence of NPs conjugated to the antibody specific for the target, the NP physical properties[36, 37] influence the test signal.[23, 29] Consequently, understanding and controlling the NP properties in these complex sample environments is critical for improving paper assay performance.

Here we examine the performance of a dipstick paper immunoassay test for rapid detection of *Vibrio parahaemolyticus* (Vp) in oysters. We systematically varied NP properties and running conditions for the dipsticks, and thus determined optimal conditions for detecting Vibrio (**Figure 1**). Assays were investigated directly in oyster hemolymph. We examined how NP surface chemistry, NP colloidal stability, and blocking agents on the strip all impact the paper immunoassay performance. We found that these parameters can be optimized to reduce non-specific adsorption, and consequently improve immunoassay sensitivity. The optimization of different factors has been studied in literature to improve the sensitivity in paper-based immunoassays, such as the NP size or antibody concentration used to make the sandwich immunoassay. Here we selected Au NPs of smaller sizes to avoid compromising the colloidal stability of the conjugates in this challenging biological media.[38] With increased robustness and improved signal intensity, the assay lends itself to detection of bacteria without culturing in a lab. Our findings open up more possibilities for the application of LFAs in food safety and bacterial pathogen detection.

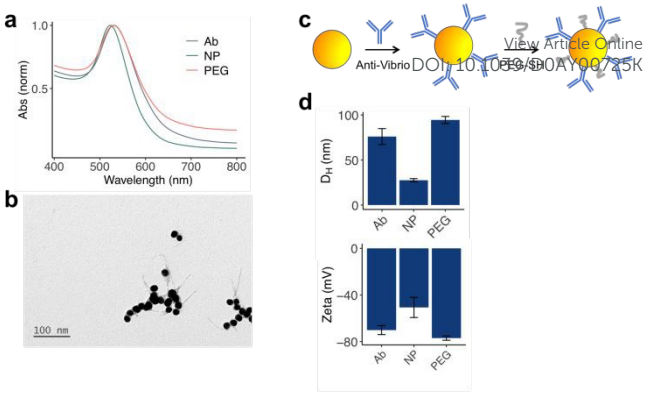

Figure 2. Antibody conjugation to Au NPs and characterization of bioconjugates. a) UV-vis spectra of bare NPs (green line) and Ab bioconjugates without and with PEG backfill (Ab –blue line- and PEG –red line- respectively). b) TEM images of the spherical gold NPs c) Schematic of the Ab conjugation strategy used in this work with PEG backfill d) Hydrodynamic diameter (D_H) and zeta potential of the unconjugated particles (NP), and Ab bioconjugates without and with PEG passivation (Ab and PEG, respectively). Error bars correspond to three independent measurements.

Results and discussion

Au NP synthesis, characterization and bioconjugation

Au NPs were synthesized following literature methods, resulting in a red colloidal solution.[39] Optical absorption spectra showed a surface plasmon resonance (SPR) of 523 nm for the bare NPs (**Figure 2a**). The morphology of the particles was investigated by TEM, which determined a mean diameter of 18.8 ± 2.5 nm (**Figure 2b**) with ImageJ. Dynamic light scattering (DLS) was used to determine the hydrodynamic diameter (D_H) of the bare particles, which was 27.5 ± 1.8 nm (upper panel, **Figure 2d**). NPs were negatively charged, with a zeta potential of -50.7 ± 8.7 mV (lower panel, **Figure 2d**).

NPs were conjugated to a polyclonal anti-vibrio antibody by electrostatic binding. The effect of NP surface modification with PEG backfill was studied by adding a thiolated mPEG (MW = 5 kDa).[40] The PEG passivates any exposed areas on the NP surface that may cause non-specific adsorption and also improves NP-Ab colloidal stability (**Figure 2c**).[40, 41] Then, the NPs were pelleted down to eliminate excess of reagents. The conjugates exhibited a redshift of the SPR of 7 and 8 nm for NP-Ab and NP-Ab + PEG, respectively. The UV-vis of the conjugates also experienced a slight broadening of the SPR peak, confirming the Ab conjugation (**Figure 2a**). Ab attachment was also verified by DLS, in which conjugates showed increased D_H of 76.1 ± 8.9 and 94.5 ± 3.9 for the conjugates without and with PEG backfill (upper panel, **Figure 2d**). Ab attachment resulted in a decrease in the surface charge of the NPs without and with surface modification leading to charges of -70.2 ± 3.9 mV and -77.1 ± 1.8 mV,

View Article Online
DOI: 10.1039/D0AY00725K

respectively (lower panel, **Figure 2d**). Altogether, these results confirm the synthesis of NP-Ab conjugates.

Running immunoassay strips

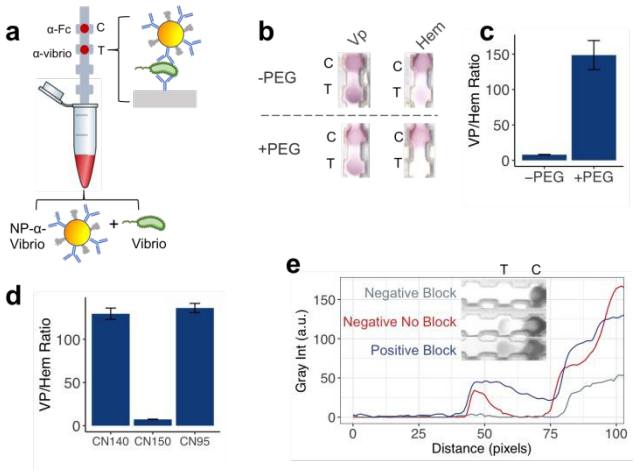

Figure 3. Strategies to eliminate false positives of the immunoassays run in hemolymph. A) schematic of the sandwich immunoassay. b) Strips run with Vp spikes (Vp) and hemolymph blanks (Hem) with the test (T) and control (C) areas shown for NP-Ab conjugates with (+PEG) and without (-PEG) PEG backfill, c) image analysis of strips in b) quantifying the test performance by the the Vp:Hem intensity ratio. Error bars correspond to three independent replicates. d) Effect of capillary speeds on the test Vp:Hem intensity ratio. Error bars correspond to three independent replicates. e) Effect of adding a nitrocellulose pretreatment step on strips (images, inset), and quantified by line scans. Gray: negative test with blocking. Red: negative test, with no blocking. Blue: positive test, with blocking.

Dipstick immunoassays were run with the filtered oyster hemolymph alone or with Vp as three independent measurements, unless specified. For Vp samples, a reference pathogenic Vp was streaked in selective agar (TCBS). A single colony was inoculated in SLB broth for 5 h at 30 °C and determined the concentration of the solution in SLB plates. Vp solutions were centrifuged and spiked into filtered hemolymph prior to running through the test. The strips with immobilized control and anti-Vibrio antibodies were immersed in the running solution, which flowed through the test by capillary action. If spots appeared at the test area, it resulted from the fact that the Vp was present and bound to both the immobilized anti-Vibrio on the nitrocellulose and the NP-anti-Vibrio, accumulating the colored NPs at the test area. If a colored spot appeared at the control area, it indicated that the immobilized anti-Fc could bind to the anti-Vibrio on the NP-anti-Vibrio conjugates, which validated that flow occurred properly in the test. Thus, if signal appeared at both the test and control areas, it was considered a positive test, while tests with a colored spot only at the control area were considered negative tests (Figure 1 and Figure 3a).

Effect of PEG backfill on immunoassays

The performance of paper immunochromatographic tests can be compromised by complex biological fluids. We have seen previous examples where the performance of the test is highly sensitive to the biological solutions used to run the tests, giving rise to false positives or false negatives.[30] Oyster hemolymph is a challenging sample matrix that impaired the performance of the tests, as it gave rise to false positives. Thus, we investigated different strategies to improve its performance.

First, we explored the effect of NP surface modification with a PEG backfill on samples run with Vp spiked in hemolymph. For NP-Ab conjugates without PEG passivation, a strong spot at the test area (T) was observed for the samples run with Vp due to formation of a sandwich immunoassay. The presence of a second spot at the control area (C) was due to immobilized anti-Fc binding to the NP-Ab conjugates, confirming the proper conjugation of the antibody and also flow in the test (upper left, **Figure 3a**). However, the control samples run in hemolymph alone also showed a faint signal at the test line, which indicated that the NP-Ab conjugates were non-specifically adsorbing to the anti-Vibrio antibody immobilized on the test line (upper right, **Figure 3a**). This constitutes a false positive result, and can be attributed to non-specific adsorption of the NP-Ab conjugate on the test area.

In comparison, color at the test line was not evident for NP-Abs that had the PEG backfill treatment when Vp was absent (lower right, **Figure 3a**), but still remained when Vp was present (lower left, **Figure 3a**). This suggested that PEG backfill reduced non-specific adsorption without compromising the test signal when Vp was present. To quantify this effect, the gray intensity of the test area was measured with ImageJ for tests spiked with Vp in hemolymph (Vp) and those run with hemolymph alone (Hem). The ratio of Vp:Hem intensity was calculated for both conditions, i.e. with and without mPEG passivation (**Figure 3b**). Surface modification of NPs allowed the increase of the Vp:Hem average ratio from 8.0 to 148.6. This confirmed that the surface chemistry modification with mPEG prevented non-specific binding of NPs at the test line, and could remove the false positive.[40]

Effect of type of nitrocellulose

We next examined the effect of changing the flow rate of the solution through the test by using nitrocelluloses with different capillary speeds. Nitrocellulose strips with capillary speeds of 65-115 (CN95), 95-155 (140) and 90-180 (150) s/40 mm were studied. Tests were run in each nitrocellulose type with hemolymph alone or with spiked Vp at 1.75 X 10^7 CFU/mL and resulting Vp:Hem gray intensity ratios were measured. The nitrocellulose with higher flow rates (CN150) led to the lowest Vp:Hem ratio compared to the other two strips with slower flow rates ($p < 0.05$) (**Figure 3c**). No statistical significant difference was observed between the nitrocelluloses CN140 and CN95. This indicated that the nitrocellulose speed rate can be tuned to optimize the visual outcomes of immunochromatographic tests. Moving forward, we used CN140 as the nitrocellulose substrate.

Effect of strip blocking

We also studied the role of blocking the strip by adding a pretreatment with Bovine Serum Albumin (BSA), which is used often to reduce non-specific adsorption to nitrocellulose. After antibody immobilization, strips were left to dry for at least half an hour. The strips were blocked by first running a 0.1% BSA solution and then were left to completely dry overnight at

View Article Online
DOI: 10.1039/D0AY01725K

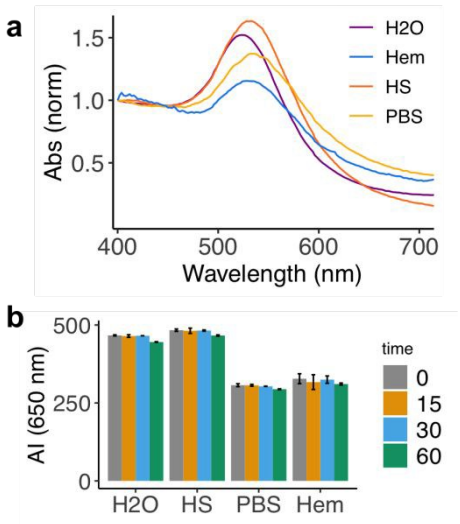

Figure 4. Study of colloidal stability in hemolymph and reference solutions. a) Uv vis spectra of NP-Ab conjugates in hemolymph (Hem, blue), human serum (HS, orange), 1X PBS (yellow), and water (Wat, purple) at the 1 h timepoint. b) Aggregation Index of the NP-Ab conjugates over time in different solutions: water (Wat), human serum (HS), PBS, and hemolymph (Hem). Error bars are obtained from two independent optical absorbance measurements.

room temperature. Strips with and without this pretreatment were then run in filtered hemolymph with or without Vp spikes. For strips without the BSA pretreatment, we observed a slight test line intensity when no Vp was present in the sample (red line, **Figure 3d**). As bioconjugates did not bind to the nitrocellulose outside of the test and control area, this indicated that the immunoprobes were non-specifically adsorbed on the immobilized antibodies at the test area. Line scans were measured with ImageJ to visualize the gray intensity signal of the tests. The false positives were not present for tests with the BSA blocking step (gray line, **Figure 3d**). Apparently, blocking reduced the electrostatic adsorption of the NP-Ab conjugates to the immobilized antibodies, favoring Ab-recognition driven interactions. When Vp was present (blue line, **Figure 3d**), signal appeared at the test and control areas, confirming a positive test. Thus, from this point, 0.1 % BSA blocked strips were used for the detection of Vp in hemolymph.

Colloidal stability of NP-Ab conjugates in hemolymph

To better understand the phenomena behind false positives in the bacterial assay, we explored the colloidal stability of the NP-Ab probes in hemolymph. To that end, we measured the optical spectra of the NPs suspended in reference buffers and in hemolymph. HS was included as a reference as it is known to stabilize the colloidal solution and prevent the presence of false positives due to the formation of a protein corona.[30] In contrast, PBS was included as a reference buffer as it is known to destabilize the colloidal suspension and induce aggregation, which leads to the formation of false positives. NPs suspended in PBS (yellow) and hemolymph (blue) led to a broader peak compared to bare NPs in water (purple), indicating that the NPs were unstable in these solutions (**Figure 4a**). For NPs suspended in HS (orange, **Figure 4a**) the SPR broadening and shift was smaller in comparison. To quantify the NP stability, an aggregation index (AI) was obtained from the UV-vis

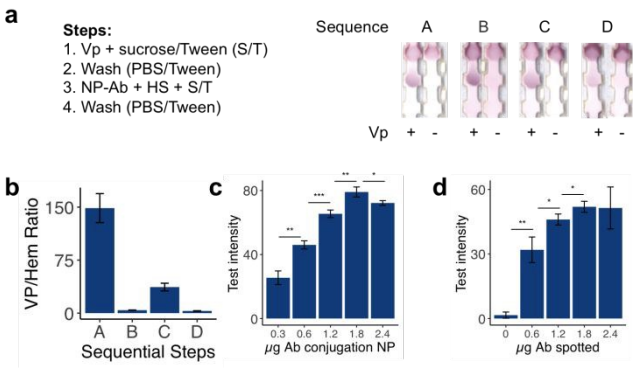

Figure 5. Improving the visual signal of the immunoassay test line when run with a reference Vp. a) Effect of running the paper-based test in sequential steps for Vp spikes into hemolymph (+) and hemolymph controls (-). For strip A, all steps of bacteria, sucrose-Tween, NP-Ab, and PBS-Tween wash were separated. For strip B, the last washing step was omitted. For strip C, the first washing step was omitted. For strip D, all solutions were combined, i.e., it was run with a single solution with HS, Vp, sucrose-Tween, and NP-Ab. b) Vp:Hem ratio of the strips for treatments A, B, C, and D. c) Selection of best Ab:NP ratio for Ab conjugation to NPs. d) Selection of optimal Ab amount immobilized on the nitrocellulose. Error bars correspond to three independent assays. P value calculated, where P***<0.001; P** < 0.01; P* < 0.05.

spectra.[41, 42] The AI was determined by calculating the area under the curve of each individual UV-vis spectrum measured from 400 to 700 nm divided by the absorption value at 650 nm. Therefore, higher AI values indicate higher colloidal stability due to a less broadened peak. NPs suspended in HS and PBS 1X buffer led to the highest and lowest AIs, respectively (**Figure 4b**). NPs suspended in hemolymph led to an AI that was lower than the NPs in water (H2O) and HS, and was comparable to NPs in PBS (**Figure 4b**). Optical absorption spectra were measured from 0 to 60 min, which allowed monitoring of NP stability with time. In all cases, the AIs decreased with time, suggesting that the NPs were destabilizing. These experiments confirm that the colloidal stability in hemolymph was affected to the same extent as in PBS, as it also has a high salt content. Altogether, the strategies followed in **Figure 3** enabled to overcome the challenges of colloidal instability triggered by hemolymph to obtain a test that can be used to detect bacteria directly in this biological fluid.

Effect of running immunoassay in sequential steps

We studied the effect of running the samples in sequential steps to optimize the visual signal of the tests (**Figure 5**). Step 1 was running the strip with 30 µL of Vp spiked in hemolymph at 1.70 X10^5 CFU/mL mixed with 12 µL of the sucrose-Tween solution (4 µL 50% w/v sucrose in water and 8 µL of 1% v/v Tween 20 in 1X PBS). This first step allowed the bacteria in solution to flow through the test by capillary action and be captured at the test line by the immobilized antibodies. Step 2 was a washing step where 50 µL of PBS-Tween20 0.1% (PBST) was added, which served to elute any bacteria non-specifically bound to the nitrocellulose. Step 3 was running the NP-Ab,

View Article Online
DOI: 10.1039/D0AY00725K

which was a solution consisting of 30 µL of HS, 12 µL of the sucrose/tween solution and 3 µL of the bioconjugates. The HS

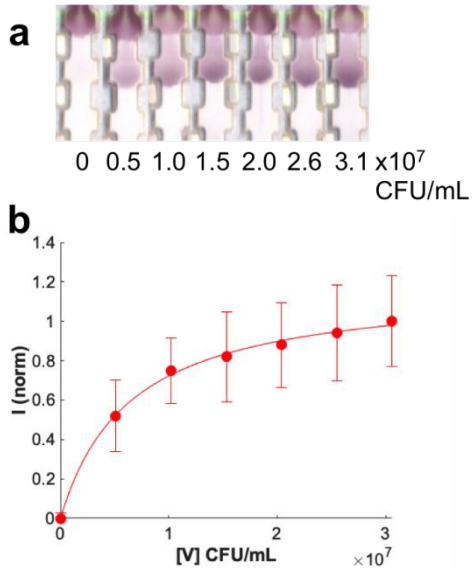

Figure 6. Limit of detection (LOD) of the optimized test run in reference Vp at different concentrations. a) Images of the dipsticks run with increasing Vp amounts. b) Normalized gray intensities at different concentrations fitted in a Langmuir-like curve (R^2 0.998), LOD = 4.66 X 10^5 CFU/mL. Error bars correspond to measurements from five independent strips.

generates a protein corona around the NP-Ab conjugates that prevents non-specific interactions. Step 4 was a final wash with 50 µL of the PBST solution to remove NPs adsorbed to the nitrocellulose. For strip A, steps 1-4 were performed separately. For strip B the washing step 4 was omitted, and for strip C, washing step 2 was omitted. Finally, strip D was run with steps 1-4 combined, i.e., a single solution of 30 µL of HS, 30 µL Vp, 12 µL of sucrose-tween and 3 µL of NP-Ab.

Vp or hemolymph alone was run in these four different sequences to the steps. The gray intensity at the test area for both positive and negative samples varied depending on the sequence of steps (**Figure 5a**). The measured Vp:Hem ratios of the test areas for each of the strips was measured (**Figure 5b**). The lowest Vp:Hem ratio was obtained for those strips that did not have the last washing step (strips B and D), which indicated that this last washing step is critical to improve the difference between positive and negative samples. Strip A achieved the best results, increasing the Vp:Hem ratio by 47.9X and 4.0X compared to the sequences D and C, respectively. This is most likely due to the separation of the bacteria capture step from the NP-Ab binding with a washing step in between, which removes bacteria electrostatically bound outside of the test area. As a result, the interaction of NP-Ab conjugates with bacteria solely captured at the test area is favored. The last washing step also improved the test performance as evidenced by the higher Vp:Hem ratio, where strip A had a Vp:Hem ratio 35.4X that of strip B (**Figure 5b**). Altogether, sequential steps allowed the improvement of the visual signal of the test. Separating these steps also reduced the time that the NP-Ab conjugates sat together in solution with the bacteria, which could potentially induce precipitation and thus decrease test line signal (**Figure 5a**, strip D). While running the tests in sequential steps increased the sample to answer time to 2 hrs, no sample preparation or bacteria culturing would be required in a laboratory, which allows to use the test on-site for Vp detection. Sequential steps could obtain a better Vp to hemolymph ratio, which has a direct impact on test sensitivity.

Effect of Ab concentration in incubation ratio

The visual signal was further improved by studying the optimal amount of capture and detection antibodies. First, NP-Ab conjugates were synthesized with different Ab coverages, which was achieved by varying the amount of Ab used in the NP-Ab conjugation from 0.3 to 2.4 µg for a fixed NP concentration. The NP-Ab conjugates were run in solutions of hemolymph with Vp spiked at 1.70 X10^5 CFU/mL. The Ab immobilized on the test line was fixed at 1.2 µg and the strips were pretreated with BSA 0.1 %. Tests were run with all steps in sequence (i.e., strip A) and gray intensity values were measured with ImageJ on the dried tests. Test line gray intensity increased with increasing Ab in the NP-Ab conjugation, and peaking at an Ab concentration of 1.8 µg (**Figure 5c**). Higher Ab coverages apparently facilitated formation of sandwich immunoassays, leading to higher retention of the immunoprobes at the test area. Increasing Ab concentration to 2.4 µg did not further improve test line intensity. Therefore, the optimal Ab conjugation was selected to determine the LOD of the designed test.

Effect of concentration of immobilized antibody

Similarly, we then explored the immobilized antibody required to obtain the highest test area intensity. The anti-vibrio species antibody was spotted on the nitrocellulose with increasing amounts ranging from 0 to 2.4 µg, and left to dry for at least 30 min before blocking the strips with BSA 0.1%. Tests were run with Vp in hemolymph at 1.70 X10^5 CFU/mL and the Ab concentration in the NP-Ab conjugation was fixed at 0.6 µg. Test line intensity increased with immobilized Ab, until saturating at 1.8 µg ($p < 0.05$) (**Figure 5d**). These results indicate that the optimal amount of immobilized Ab is 1.8 µg and higher amounts do not improve signal significantly.

Limit of detection

Once optimal parameters for the test were determined, we measured the LOD of the assay. The reference Vp from ATCC was spiked in hemolymph at concentrations ranging from 0 to 3.06 X 10^7 CFU/mL and the test was run using optimal conditions. In short, Ab-NP conjugation was done at 1.8 µg and a PEG backfill surface modification was used. The antibody was spotted at 1.8 µg on the nitrocellulose CN140 and blocked with BSA 0.1%. Tests were run with a sequence A, which ran the assay in four steps that consisted of first capturing the bacteria at the test line, washing the non-specifically bound bacteria, retaining the NP-Ab conjugates and finally washing the strips to reduce non-specific binding. Gray intensities at the test area increased with higher bacteria concentrations (**Figure 6a**). Intensity values were fit to a modified Langmuir curve to determine the LOD (Materials and Methods). The LOD obtained was 4.66 X 10^5 CFU/mL (R^2 = 0.998) (**Figure 6b**). This LOD is below the reported Vp dose with a 50% probability to

cause a food borne infection (ID_{50}), and thus the assay has the potential to be used as a point of care diagnostic.[5]

Conclusions

In this work, we developed a paper immunoassay suitable for detecting Vp directly from oyster hemolymph. Sample matrix issues posed a significant challenge, where the hemolymph reduced the colloidal stability of the NP probes, impairing the performance of the assay. NP-Ab behavior in hemolymph was similar to that in PBS, where the high salinity caused non-specific adsorption and resulted in false positives. While the sample matrix can be challenging to work with, we explored different strategies to improve the stability of the NP-Ab conjugate via surface chemistry modifications or the formation of a HS protein corona. [30] In addition, blocking conditions for the nitrocellulose assay were used to avoid non-specific interactions. Running fluids sequentially through the strip also facilitated proper sandwich formation at the test line by minimizing opportunities for NP-Ab aggregation and bacterial non-specific adsorption. While separating steps lengthens overall sample to answer time to ~2 hrs, the optimized test allows the detection of Vp without taking back a sample to a lab for culturing and bacterial identification. Utilizing these strategies, the paper immunoassay detected Vp at levels relevant for infection. Arriving at optimal conditions could also be achieved using an orthogonal method. Additional optimization strategies can be addressed towards the mass-production of these tests for their commercialization, such as the use of laser inks to immobilize the Abs on the nitrocellulose as a test line, and changing test area dimensions to lines instead of spots to concentrate the signal. In addition, other routes to enhance the signal in paper immunoassays such as surface enhanced Raman spectroscopy tags, [43, 44] isotachophoresis, [45] and photothermal heating [46] all can be combined with this approach. Ultimately, these results will aid in using paper immunoassays for various food safety applications. Critical to this would be comparison of the assay against gold standards in field experiments.

Experimental

Reagents

Gold chloride ($HAuCl_4 \cdot 3H_2O$) (99.9%) (CAS: 16961-25-4), sucrose (CAS: 57-50-1), bovine serum albumin (BSA) (CAS: 9048-46-8), Tween-20 (CAS: 9005-64-5), trisodium citrate (Na3C6H5O7) (CAS: 6132-04-3), HEPES ($C_8H_{18}N_2S$) (≥99.5%) (CAS 7365-45-9), Serum from human male AB plasma sterile-filtered, Anti-Rabbit IgG (Fc), Gel blotting paper used as absorbant pad (GB003 Gel Blot paper) were all purchased from Sigma. Polyclonal anti-vibrio species antibody was purchased from Seracare. UniStart Nitrocellulose CN95, CN140 and CN150 with plastic backing was purchased from Sartorius. The backing paper (MIBA-010 Backing Card, 0.020" thickness) was purchased through DCN Diagnostics. 5kD mPEG was purchased from nanocs. Phosphate Buffer Saline (1X PBS, pH 7.4) was purchased from Gibco. Tryptone Peptone was purchased from Gibco. Sodium chloride (≥ 99%) (CAS: 7647-14-5), was purchased from Honeywell. Technical agar solidifying agent, technical yeast extract and TCBS Agar were purchased from Difco. Vp was obtained from ATCC 17802™.

Gold NP Synthesis

Spherical gold nanoparticles (Au NPs) were synthesized by citrate reduction of gold chloride.[39] A 50 mL solution of $HAuCl_4 \bullet 3H_2O$ at 0.25 mM was brought to boil and 1 mL of sodium citrate 6.8 mM was added to the boiling solution for 15 minutes under stirring to form the gold NPs. The NP solution was left to cool down until room temperature was reached.

Gold NP Characterization

Optical absorption spectra were measured on an Agilent Cary 5000 UV-Vis-NIR spectrometer from 400 to 800 nm. To address simultaneously the stability of the NPs suspended in different concentrations over time, the plate reader (Molecular Devices) was used instead. Images of the NPs were obtained with TEM (FEI Tecnai G2 at 120 kV) and size quantification from these images was measured with ImageJ (Version 2.0.0). The hydrodynamic diameter (D_H) and zeta potential of the particles were measured with a Nanoparticle Analyzer SZ-100 from Horiba.

Calculation of the Aggregation Index

The stability of the NPs in different solutions was determined from their optical absorption spectra by the aggregation index (AI). The AI value was calculated as the area under the curve of the absorption spectra from 400 to 700 nm, divided by the intensity at 650 nm. High AI values corresponded to more stable particles.

Antibodies

Electrostatic binding was used for bioconjugation of the polyclonal anti-vibrio antibody to the NPs. The pellet from 1 mL of NPs was centrifuged at 12000 g for 12 min and resuspended in 300 µL of Milli-Q water (18 MΩ.cm), 100 µL of HEPES 40 mM pH 7.7 and 5 µL of anti-vibrio antibody at 1 mg/mL (unless specified). The solution was left overnight with gentle agitation at room temperature. For those experiments where PEG backfill was incorporated into the synthesis, 10 µL of 0.1 mM mPEG (MW 5000 Da) were added to the solution and left for 15 min to allow the PEG to passivate the NP surface.[47] The particles were then concentrated to a 25 µL pellet by centrifugation at 8000 g for 12 min.

Paper strip immunoassays

Dipsticks consisted of two parts: a laser-cut UniStar nitrocellulose of different capillary speeds (CN95, CN140, CN150) and an adsorbent pad that acted as a wick. The wick had dimensions of 7.1 x 0.5 cm to ensure the complete absorption of all of the solutions used in the test. Both parts were assembled together with the help of a backing paper. Antibodies were manually spotted on the nitrocellulose in 0.3 µL aliquots to obtain 1.2 µg of antibody spotted if not specified. Two antibodies were used, the anti-vibrio antibody on the test area and an anti-IgG-Fc antibody on the control area. For the nitrocellulose pre-treatment, a blocking step was

added by running 50 µL of BSA 0.1% and left to dry overnight. Tests were run in three independent replicates with the following sequential steps, unless otherwise specified. First, 30 µL of bacteria spiked in filtered hemolymph was run with 12 µL of a sucrose-tween mixture (4 µL 50% w/v sucrose in water and 8 µL of 1% v/v Tween 20 in PBS 1X). An intermediate washing step with 50 µL of PBS-Tween20 0.1% (PBST) was added previously to running the nanoparticle mixture, which consisted on a solution of 30 µL of human serum (HS), 12 µL sucrose-tween and 3 µL of the NP pellet. Finally, a last washing step was added with 50 µL of PBST. The strips were left to dry at room temperature and scanned for quantification.

Image analysis

Images were analyzed with ImageJ for quantification[48]. The gray intensity of the background was subtracted from the test area for each nitrocellulose. For determination of the Vp to hemolymph ratio, the gray value on the test area for the samples run with Vp at a known concentration was divided by the strip run in hemolymph alone. For determination of the LOD, the strips were run in five independent replicates at different antigen concentrations and normalized using the equation;

$$I = \frac{I_n - I_m}{I_M - I_m}$$

where I_n was the gray value of the test area at a given concentration and I_M and I_m were the maximum and minimum intensity measured for all the tests, respectively. The normalized values were then fitted with a Langmuir-like equation and the limit of detection (LOD) was determined as the concentration that exceeded three times the value of the standard deviation of the negative control, i.e. samples run in hemolymph alone.

Oyster hemolymph

Oysters were obtained from commercial sources, shucked and hemolymph extracted with a micropipette. Typically, 2-10 mL of hemolymph were extracted per oyster. The hemolymph pool was then filtered through 0.22 µm to eliminate bacteria present in the samples and kept at -20 °C until used.

Vibrio growth

A reference pathogenic strain of Vp (ATCC 17802) was used to optimize this test. Bacteria were streaked in selective agar media, thiosulfate citrate bile salts sucrose agar (TCBS), and a single colony was inoculated in SLB broth under sterile conditions. This solution was left to grow at 30 °C for 5 h and used as a mother solution to generate fresh aliquots. A 10 µL inoculum from this sample was grown in SLB broth for 5 h at 30 °C and spiked in filtered hemolymph by pelleting down the bacteria at 3000 rpm for 20 min. Concentration was determined by spreading evenly 50 µL of a 1:100,000 dilution in SLB plates and left overnight at 30 °C for single colony count.

Conflicts of interest

There are no conflicts to declare.

Acknowledgements

View Article Online
DOI: 10.1039/D0AY00725K

This work was supported by from Canon Virginia Inc. and MIT SeaGrant. CRQ was supported by a fellowship from the Rafael del Pino foundation, the UMass Boston College of Science and Mathematics Dean's Doctoral Research Fellowship from Oracle, and the UMass Boston Beacon Student Success Fellowship.

Notes and references

1. M. F. Tlusty, *Frontiers in Ecology and the Environment*, 2013, **11**, 121-122.
2. G. D. Stentiford, D. M. Neil, E. J. Peeler, J. D. Shields, H. J. Small, T. W. Flegel, J. M. Vlak, B. Jones, F. Morado, S. Moss, J. Lotz, L. Bartholomay, D. C. Behringer, C. Hauton and D. V. Lightner, *Journal of Invertebrate Pathology*, 2012, **110**, 141-157.
3. Y. Zhao, H. Wang, P. Zhang, C. Sun, X. Wang, X. Wang, R. Yang, C. Wang and L. Zhou, *Scientific Reports*, 2016, **6**, 21342.
4. R. E. Hartnell, L. Stockley, W. Keay, et al., *International Journal of Food Microbiology*, 2019, **288**, 58-65.
5. *Quantitative Risk Assessment on the Public Health Impact of Pathogenic Vibrio parahaemolyticus In Raw Oysters*, Food and Drug Administration, 2005.
6. E. Scallan, R. M. Hoekstra, F. J. Angulo, R. V. Tauxe, M.-A. Widdowson, S. L. Roy, J. L. Jones and P. M. Griffin, *Emerg Infect Dis*, 2011, **17**, 7-15.
7. J. Martinez-Urtaza, J. C. Bowers, J. Trinanes and A. DePaola, *Food Research International*, 2010, **43**, 1780-1790.
8. Y. Liu, Z. Zhang, Y. Wang, Y. Zhao, Y. Lu, X. Xu, J. Yan and Y. Pan, *International Journal of Food Microbiology*, 2015, **211**, 109-116.
9. P. Prompamorn, P. Sithigorngul, S. Rukpratanporn, S. Longyant, P. Sridulyakul and P. Chaivisuthangkura, *Letters in Applied Microbiology*, 2011, **52**, 344-351.
10. E. Morales-Narváez, T. Naghdi, E. Zor and A. Merkoçi, *Analytical Chemistry*, 2015, **87**, 8573-8577.
11. L. Russo, J. Leva Bueno, J. F. Bergua, M. Costantini, M. Giannetto, V. Puntes, A. de la Escosura-Muñiz and A. Merkoçi, *ACS Omega*, 2018, **3**, 18849-18856.
12. Y. Zhao, G. Zhang, Q. Liu, M. Teng, J. Yang and J. Wang, *Journal of Agricultural and Food Chemistry*, 2008, **56**, 12138-12142.
13. C. L. Mthembu, M. I. Sabela, M. Mlambo, L. M. Madikizela, S. Kanchi, H. Gumede and P. S. Mdluli, *Analytical Methods*, 2017, **9**, 5943-5951.
14. Z. Li, M. You, Y. Bai, Y. Gong and F. Xu, *Small Methods*, 2019, **n/a**, 1900459.
15. Y. Gong, Y. Zheng, B. Jin, M. You, J. Wang, X. Li, M. Lin, F. Xu and F. Li, *Talanta*, 2019, **201**, 126-133.
16. F. Li, M. You, S. Li, J. Hu, C. Liu, Y. Gong, H. Yang and F. Xu, *Biotechnology Advances*, 2020, **39**, 107442.
17. M. You, M. Lin, Y. Gong, S. Wang, A. Li, L. Ji, H. Zhao, K. Ling, T. Wen, Y. Huang, D. Gao, Q. Ma, T. Wang, A. Ma, X. Li and F. Xu, *ACS Nano*, 2017, **11**, 6261-6270.
18. D. R. Hristov, C. Rodríguez-Quijada, J. Gomez-Marquez and K. Hamad-Schifferli, *Sensors*, 2019, **19**, 554.
19. S. M. Z. Hossain, C. Ozimok, C. Sicard, S. D. Aguirre, M. M. Ali, Y. Li and J. D. Brennan, *Analytical and Bioanalytical Chemistry*, 2012, **403**, 1567-1576.

20. J. Hwang, S. Lee and J. Choo, *Nanoscale*, 2016, **8**, 11418-11425.
21. G. A. Posthuma-Trumpie, J. Korf and A. van Amerongen, *Analytical and Bioanalytical Chemistry*, 2009, **393**, 569-582.
22. W. Ren, D. R. Ballou, R. FitzGerald and J. Irudayaraj, *Biosensors and Bioelectronics*, 2019, **126**, 324-331.
23. D. Quesada-González and A. Merkoçi, *Biosensors and Bioelectronics*, 2015, **73**, 47-63.
24. H. Kim, D.-R. Chung and M. Kang, *Analyst*, 2019, **144**, 2460-2466.
25. A. W. Martinez, S. T. Phillips, G. M. Whitesides and E. Carrilho, *Analytical Chemistry*, 2009, **82**, 3-10.
26. X. Ge, A. M. Asiri, D. Du, W. Wen, S. Wang and Y. Lin, *TrAC Trends in Analytical Chemistry*, 2014, **58**, 31-39.
27. L. P. Murray, K. R. Baillargeon, J. R. Bricknell and C. R. Mace, *Analytical Methods*, 2019, **11**, 930-935.
28. M. D. Kulinski, M. Mahalanabis, S. Gillers, J. Y. Zhang, S. Singh and C. M. Klapperich, *Biomedical Microdevices*, 2009, **11**, 671-678.
29. H. de Puig Guixé, I. Bosch, L. Gehrke and K. Hamad-Schifferli, *Trends in Biotechnology*, 2017, **35**, 1169-1180.
30. H. de Puig, I. Bosch, M. Carre-Camps and K. Hamad-Schifferli, *Bioconjugate Chemistry*, 2017, **28**, 230-238.
31. J. O. Tam, H. de Puig, C.-w. Yen, I. Bosch, J. Gómez-Márquez, C. Clavet, K. Hamad-Schifferli and L. Gehrke, *Journal of Immunoassay and Immunochemistry*, 2017, **38**, 355-377.
32. X. Zhang, Z. Sun, X. Zhang, M. Zhang and S. Li, *Applied and Environmental Microbiology*, 2018, **84**, e02824-02817.
33. S. A. Walper, G. Lasarte Aragonés, K. E. Sapsford, C. W. Brown, C. E. Rowland, J. C. Breger and I. L. Medintz, *ACS Sensors*, 2018, **3**, 1894-2024.
34. B. O'Farrell, in *Lateral Flow Immunoassay*, eds. R. Wong and H. Tse, Humana Press, Totowa, NJ, 2009, DOI: 10.1007/978-1-59745-240-3_1, pp. 1-33.
35. L. S. A. Busa, S. Mohammadi, M. Maeki, A. Ishida, H. Tani and M. Tokeshi, *Micromachines*, 2016, **7**, 86.
36. C. J. Murphy, A. M. Gole, J. W. Stone, P. N. Sisco, A. M. Alkilany, E. C. Goldsmith and S. C. Baxter, *Accounts of Chemical Research*, 2008, **41**, 1721-1730.
37. X. Huang, R. O'Connor and E. A. Kwizera, *Nanotheranostics*, 2017, DOI: 10.7150/ntno.18216.
38. Y. Gong, J. Hu, J. R. Choi, M. You, Y. Zheng, B. Xu, T. Wen and F. Xu, *Int J Nanomedicine*, 2017, **12**, 4455-4466.
39. J. Turkevich, P. C. Stevenson and J. Hillier, *Discussions of the Faraday Society*, 1951, **11**, 55-75.
40. Q. Dai, C. Walkey and W. C. W. Chan, *Angewandte Chemie International Edition*, 2014, **53**, 5093-5096.
41. H. de Puig, S. Federici, S. H. Baxamusa, P. Bergese and K. Hamad-Schifferli, *Small*, 2011, **7**, 2477-2484.
42. J. C.-Y. Kah, A. Zubieta, R. A. Saavedra and K. Hamad-Schifferli, *Langmuir*, 2012, **28**, 8834-8844.
43. M. Sanchez-Purra, M. Carre Camps, H. de Puig Guixé, I. Bosch, L. Gehrke and K. Hamad-Schifferli, *ACS Infectious Diseases*, 2017, **2**, 401-409.
44. M. Sánchez-Purrà, B. Roig-Solvas, A. Versiani, C. Rodriguez-Quijada, H. de Puig, I. Bosch, L. Gehrke and K. Hamad-Schifferli, *Molecular Systems Design & Engineering*, 2017, **2**, 401-409.
45. K. T. C. Babak Y. Moghadam, and Jonathan D. Posner, *Analytical Chemistry*, 2015, **87**, 1009-1017.
46. Z. Qin, W. C. W. Chan, D. R. Boulware, T. Akkin, E. K. Butler and J. C. Bischof, *Angewandte Chemie International Edition*, 2012, **51**, 4358-4361.
47. C.-W. Yen, H. de Puig, J. Tam, J. Gómez-Márquez, I. Bosch, K. Hamad-Schifferli and L. Gehrke, *Lab on a Chip*, 2015, **15**, 1638-1641.
48. M. D. Abramoff, P. J. Magelhaes and S. J. Ram, *Biophotonics International*, 2004, **11**, 36-42.

1

View Article Online
DOI: 10.1039/D0AY00725K

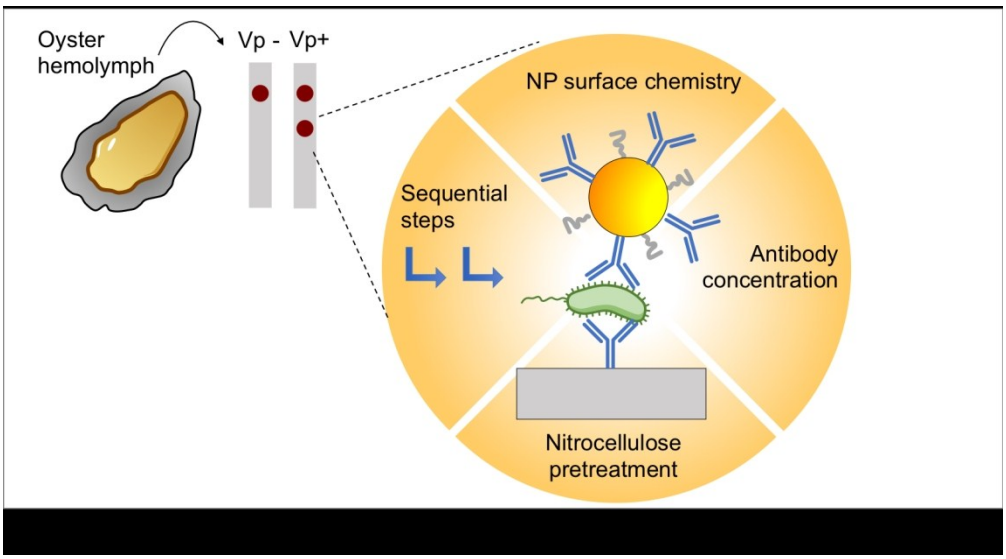

We develop a dipstick paper immunoassay for Vibrio parahaemolyticus using gold nanoparticle-antibody conjugates and determine optimal running conditions.